Chapter 2
A Progressive Asymptotic Approach Procedure for Simulating Steady-State Natural Convective Problems in Fluid-Saturated Porous Media

In a fluid-saturated porous medium, a change in medium temperature may lead to a change in the density of pore-fluid within the medium. This change can be considered as a buoyancy force term in the momentum equation to determine pore-fluid flow in the porous medium using the Oberbeck-Boussinesq approximation model. The momentum equation used to describe pore-fluid flow in a porous medium is usually established using Darcy's law or its extensions. If a fluid-saturated porous medium has the geometry of a horizontal layer, and is heated uniformly from the bottom of the layer, then there exists a temperature difference between the top and bottom boundaries of the layer. Since the positive direction of the temperature gradient due to this temperature difference is opposite to that of the gravity acceleration, there is no natural convection for a small temperature gradient in the porous medium. In this case, heat energy is solely transferred from the high temperature region (the bottom of the horizontal layer) to the low temperature region (the top of the horizontal layer) by thermal conduction. However, if the temperature difference is large enough, it may trigger natural convection in the fluid-saturated porous medium. This problem was first treated analytically by Horton and Rogers (1945) as well as Lapwood (1948), and is often called the Horton-Rogers-Lapwood problem.

This kind of natural convection problem has been found in many geoscience fields. For example, in geoenvironmental engineering, buried nuclear waste and industrial waste in a fluid-saturated porous medium may generate heat and result in a temperature gradient in the vertical direction. If the Rayleigh number, which is directly proportional to the temperature gradient, is equal to or greater than the critical Rayleigh number, natural convection will take place in the porous medium, so that the groundwater may be severely contaminated due to the pore-fluid flow circulation caused by the natural convection. In geophysics, there exists a vertical temperature gradient in the Earth's crust. If this temperature gradient is large enough, it will cause regional natural convection in the Earth's crust. In this situation, the pore-fluid flow circulation due to the natural convection can dissolve soluble minerals in some part of a region and carry them to another part of the region. This is the mineralization problem closely associated with geophysics and geology. Since a natural porous medium is often of a complicated geometry and composed of many

C. Zhao et al., *Fundamentals of Computational Geoscience*,
Lecture Notes in Earth Sciences 122, DOI 10.1007/978-3-540-89743-9_2,

different materials, numerical methods are always needed to solve the aforementioned problems.

From the mathematical point of view, the Horton-Rogers-Lapwood problem possesses a bifurcation. The linear stability theory based on the first-order perturbation is commonly used to solve this problem analytically and numerically (Nield 1968, Palm et al. 1972, Caltagirone 1975, 1976, Combarnous and Bories 1975, Buretta and Berman 1976, McKibbin and O'Sullivan 1980, Kaviany 1984, Lebon and Cloot 1986, Pillatsis et al. 1987, Riley and Winters 1989, Islam and Nandakumar 1990, Phillips 1991, Nield and Bejan 1992, Chevalier et al. 1999). However, Joly et al. (1996) pointed out that: "The linear stability theory, in which the nonlinear term of the heat disturbance equation has been neglected, does not describe the amplitude of the resulting convection motion. The computed disturbances are correct only for infinitesimal amplitudes. Indeed, even if the form of convective motion obtained for low supercritical conditions is often quite similar to the critical disturbance, the nonlinear term may produce manifest differences, especially when strong constraints, such as impervious or adiabatic boundaries, are considered." Since it is the amplitude and the form of natural convective motion that significantly affects or dominates the contaminant transport and mineralization in a fluid-saturated porous medium, there is a definite need for including the full nonlinear term of the energy equation in the finite element analysis.

From the finite element analysis point of view, the direct inclusion of the full nonlinear term of the energy equation in the steady-state Horton-Rogers-Lapwood problem would result in a formidable difficulty. The finite element method needs to deal with a highly nonlinear problem and often suffers difficulties in establishing the true non-zero velocity field in a fluid-saturated porous medium because the Horton-Rogers-Lapwood problem always has a zero solution as one possible solution for the velocity field of the pore-fluid. If the velocity field of the pore-fluid used at the beginning of an iteration method is not chosen appropriately, then the resulting finite element solution always tends to zero for the velocity field in a fluid-saturated porous medium. Although this difficulty can be circumvented by turning a steady-state problem into a transient one (Trevisan and Bejan 1987), it is often unnecessary and computationally inefficient to obtain a steady-state solution from solving a transient problem. Therefore, it is highly desirable to develop a numerical procedure to directly solve the steady-state Horton-Rogers-Lapwood problem. For this reason, a progressive asymptotic approach procedure has been developed in recent years (Zhao et al. 1997a, 1998a). The developed progressive asymptotic approach procedure is based on the concept of an asymptotic approach, which was previously and successfully applied to some other fields of the finite element method. For instance, the h-adaptive mesh refinement (Cook et al. 1989) is based on the asymptotic approach concept and can produce a satisfactory solution with the progressive reduction in the size of finite elements used in the analysis. The same asymptotic approach concept was also employed to obtain asymptotic solutions for natural frequencies of vibrating structures in a finite element analysis (Zhao and Steven 1996a, b, c). To solve the steady-state Horton-Rogers-Lapwood problem with the full nonlinear term of the energy equation included in the finite

element analysis, the asymptotic approach concept needs to be combined with the finite element method in a different fashion (Zhao et al. 1997a).

2.1 Governing Equations of the Problem

For a two-dimensional fluid-saturated porous medium, if Darcy's law is used to describe pore-fluid flow and the Oberbeck-Boussinesq approximation is employed to describe a change in pore-fluid density due to a change in pore-fluid temperature, the governing equations of a natural convection problem, known as the steady-state Horton-Rogers-Lapwood problem (Nield and Bejan 1992, Zhao et al. 1997a), for incompressible pore-fluid can be expressed as

$$\frac{\partial u}{\partial x} + \frac{\partial v}{\partial y} = 0, \tag{2.1}$$

$$u = \frac{K_x}{\mu}\left(-\frac{\partial P}{\partial x} + \rho_f g_x\right), \tag{2.2}$$

$$v = \frac{K_y}{\mu}\left(-\frac{\partial P}{\partial y} + \rho_f g_y\right), \tag{2.3}$$

$$\rho_{f0} c_p \left(u\frac{\partial T}{\partial x} + v\frac{\partial T}{\partial y}\right) = \lambda_{ex}\frac{\partial^2 T}{\partial x^2} + \lambda_{ey}\frac{\partial^2 T}{\partial y^2}, \tag{2.4}$$

$$\rho_f = \rho_{f0}[1 - \beta_T(T - T_0)], \tag{2.5}$$

$$\lambda_{ex} = \phi\lambda_{fx} + (1-\phi)\lambda_{sx}, \qquad \lambda_{ey} = \phi\lambda_{fy} + (1-\phi)\lambda_{sy}, \tag{2.6}$$

where u and v are the horizontal and vertical velocity components of the pore-fluid in the x and y directions respectively; P is the pore-fluid pressure; T is the temperature of the porous material; K_x and K_y are the permeabilities of the porous material in the x and y directions respectively; μ is the dynamic viscosity of the pore-fluid; ρ_f is the density of the pore-fluid; ρ_{f0} and T_0 are the reference density and temperature; λ_{fx} and λ_{sx} are the thermal conductivities of the pore-fluid and rock mass in the x direction; λ_{fy} and λ_{sy} are the thermal conductivities of the pore-fluid and rock mass in the y direction; c_p is the specific heat of the pore-fluid; g_x and g_y are the gravity acceleration components in the x and y directions; ϕ and β_T are the porosity of the porous material and the thermal volume expansion coefficient of the pore-fluid.

It is noted that Eqs. (2.1), (2.2), (2.3) and (2.4) are derived under the assumption that the porous medium considered is orthotropic, in which the y axis is upward in the vertical direction and coincides with the principal direction of medium permeability as well as that of medium conductivity.

In order to simplify Eqs. (2.1), (2.2), (2.3) and (2.4), the following dimensionless variables are defined:

$$x^* = \frac{x}{H}, \qquad y^* = \frac{y}{H}, \qquad T^* = \frac{T - T_0}{\Delta T}, \tag{2.7}$$

$$u^* = \frac{H\rho_{f0}c_p}{\lambda_{e0}}u, \qquad v^* = \frac{H\rho_{f0}c_p}{\lambda_{e0}}v, \quad P^* = \frac{K_h\rho_{f0}c_p}{\mu\lambda_{e0}}(P - P_0), \tag{2.8}$$

$$K_x^* = \frac{K_x}{K_h}, \qquad K_y^* = \frac{K_y}{K_h}, \qquad \lambda_{ex}^* = \frac{\lambda_{ex}}{\lambda_{e0}}, \qquad \lambda_{ey}^* = \frac{\lambda_{ey}}{\lambda_{e0}}, \tag{2.9}$$

where x^* and y^* are the dimensionless coordinates; u^* and v^* are the dimensionless velocity components in the x and y directions respectively; P^* and T^* are the dimensionless excess pressure and temperature; K_h is a reference medium permeability coefficient in the horizontal direction; λ_{e0} is a reference conductivity coefficient of the porous medium; $\Delta T = T_{bottom} - T_0$ is the temperature difference between the bottom and top boundaries of the porous medium; H is a reference length and P_0 is the static pore-fluid pressure.

Substituting the above dimensionless variables into Eqs. (2.1), (2.2), (2.3) and (2.4) yields the following dimensionless equations:

$$\frac{\partial u^*}{\partial x^*} + \frac{\partial v^*}{\partial y^*} = 0, \tag{2.10}$$

$$u^* = K_x^*\left(-\frac{\partial P^*}{\partial x^*} + RaT^*e_1\right), \tag{2.11}$$

$$v^* = K_y^*\left(-\frac{\partial P^*}{\partial y^*} + RaT^*e_2\right), \tag{2.12}$$

$$u^*\frac{\partial T^*}{\partial x^*} + v^*\frac{\partial T^*}{\partial y^*} = \lambda_{ex}^*\frac{\partial^2 T^*}{\partial x^{*2}} + \lambda_{ey}^*\frac{\partial^2 T^*}{\partial y^{*2}}, \tag{2.13}$$

where $\boldsymbol{e}$ is a unit vector and $\boldsymbol{e} = e_1 i + e_2 j$ for a two-dimensional problem; Ra is the Rayleigh number, defined in this particular case as

$$Ra = \frac{(\rho_{f0}c_p)\rho_{f0}g\beta\Delta TK_hH}{\mu\lambda_{e0}}. \tag{2.14}$$

2.2 Finite Element Formulation of the Problem

By considering the dimensionless velocity, pressure and temperature as basic variables, Eqs. (2.10), (2.11), (2.12) and (2.13) can be discretized using the conventional finite element method (Zienkiewicz 1977, Zhao et al. 1997a). For a typical 4-node quadrilateral element, the velocity, pressure and temperature fields at the elemental level can be expressed as

$$u^*(x^*,\ y^*) = \boldsymbol{\varphi}^T\ \mathbf{U^e}, \tag{2.15}$$

$$v^*(x^*,\ y^*) = \boldsymbol{\varphi}^T\ \mathbf{V^e}, \tag{2.16}$$

$$P^*(x^*,\ y^*) = \boldsymbol{\Psi}^T\ \mathbf{P^e}, \tag{2.17}$$

$$T^*(x^*,\ y^*) = \boldsymbol{\varphi}^T\ \mathbf{T^e}, \tag{2.18}$$

where $\mathbf{U^e}$, $\mathbf{V^e}$, $\mathbf{P^e}$ and $\mathbf{T^e}$ are the column vectors of the nodal velocity, excess pressure and temperature of the element; $\boldsymbol{\varphi}$ is the column vector of the interpolation functions for the dimensionless velocity and temperature fields within the element; $\boldsymbol{\Psi}$ is the column vector of the interpolation functions for the excess pressure within the element. For the 4-node quadrilateral element, it is assumed that $\boldsymbol{\varphi}$ is identical to $\boldsymbol{\Psi}$ in the following numerical analysis.

The global coordinate components within the element can be defined as

$$x^* = \mathbf{N}^T\mathbf{X}, \qquad y^* = \mathbf{N}^T\mathbf{Y}, \tag{2.19}$$

where $\mathbf{X}$ and $\mathbf{Y}$ are the column vectors of nodal coordinate components in the x and y directions of the global coordinate system respectively; $\mathbf{N}$ is the column vector of the coordinate mapping function of the element. Based on the isoparametric element concept, the following relationships exist:

$$\mathbf{N}(\xi, \eta) = \boldsymbol{\varphi}(\xi, \eta) = \boldsymbol{\Psi}(\xi, \eta), \tag{2.20}$$

where ξ and η are the local coordinate components of the element.

Using the Galerkin weighted-residual method, Eqs. (2.10), (2.11), (2.12) and (2.13) can be expressed, with consideration of Eqs. (2.15), (2.16), (2.17) and (2.18), as follows:

$$\int_A \boldsymbol{\Psi}\frac{\partial \boldsymbol{\varphi}^T}{\partial x^*}\mathbf{U^e}\ dA + \int_A \boldsymbol{\Psi}\frac{\partial \boldsymbol{\varphi}^T}{\partial y^*}\mathbf{V^e}\ dA = 0, \tag{2.21}$$

$$\int_A \boldsymbol{\varphi}\boldsymbol{\varphi}^T\ \mathbf{U^e}\ dA + \int_A \boldsymbol{\varphi} K_x^* \frac{\partial \Psi^T}{\partial x^*}\mathbf{P^e}\ dA + \int_A \boldsymbol{\varphi} K_x^* Ra\boldsymbol{\varphi}^T\ \mathbf{T^e}\ e_1 dA = 0, \tag{2.22}$$

$$\int_A \boldsymbol{\varphi}\boldsymbol{\varphi}^T \, \mathbf{V^e} \, dA + \int_A \boldsymbol{\varphi} K_y^* \frac{\partial \boldsymbol{\Psi}^T}{\partial y^*} \, \mathbf{P^e} \, dA + \int_A \boldsymbol{\varphi} K_y^* Ra \boldsymbol{\varphi}^T \, \mathbf{T^e} \, e_2 dA = 0, \tag{2.23}$$

$$\int_A \boldsymbol{\varphi} u^* \frac{\partial \boldsymbol{\varphi}^T}{\partial x^*} \, \mathbf{T^e} \, dA + \int_A \boldsymbol{\varphi} v^* \frac{\partial \boldsymbol{\varphi}^T}{\partial y^*} \, \mathbf{T}^e \, dA - \int_A \boldsymbol{\varphi} \, \lambda_{ex}^* \frac{\partial^2 \boldsymbol{\varphi}^T}{\partial x^{*2}} \, \mathbf{T}^e \, dA - \int_A \boldsymbol{\varphi} \, \lambda_{ey}^* \frac{\partial^2 \boldsymbol{\varphi}^T}{\partial y^{*2}} \, \mathbf{T^e} dA = 0. \tag{2.24}$$

Using the Green-Gauss theorem and the technique of integration by parts, the terms involving the second derivatives in Eq. (2.24) can be rewritten as

$$\int_A \boldsymbol{\varphi} \, \lambda_{ex}^* \frac{\partial^2 \boldsymbol{\varphi}^T}{\partial x^{*2}} \, \mathbf{T^e} \, dA = - \int_A \frac{\partial \boldsymbol{\varphi}}{\partial x^*} \, \lambda_{ex}^* \frac{\partial \boldsymbol{\varphi}^T}{\partial x^*} \, \mathbf{T^e} \, dA + \int_S \boldsymbol{\varphi} q_x^* n_x dS = 0, \tag{2.25}$$

$$\int_A \boldsymbol{\varphi} \, \lambda_{ey}^* \frac{\partial^2 \boldsymbol{\varphi}^T}{\partial y^{*2}} \, \mathbf{T^e} \, dA = - \int_A \frac{\partial \boldsymbol{\varphi}}{\partial y^*} \, \lambda_{ey}^* \frac{\partial \boldsymbol{\varphi}^T}{\partial y^*} \, \mathbf{T^e} dA + \int_S \boldsymbol{\varphi} q_y^* n_y dS = 0, \tag{2.26}$$

where q_x^* and q_y^* are the dimensionless heat fluxes on the element boundary of a unit normal vector, $\boldsymbol{n}$; A and S are the area and boundary length of the element.

Note that Eqs. (2.21), (2.22), (2.23) and (2.24) can be expressed in a matrix form as follows:

$$\begin{bmatrix} \mathbf{M^e} & \mathbf{0} & -\mathbf{B_x^e} & -\mathbf{A_x^e} \\ 0 & \mathbf{M^e} & -\mathbf{B_y^e} & -\mathbf{A_y^e} \\ 0 & 0 & \mathbf{E^e} & 0 \\ \mathbf{C_x^e} & \mathbf{C_y^e} & 0 & 0 \end{bmatrix} \begin{Bmatrix} \mathbf{U^e} \\ V^{\mathbf{e}} \\ \mathbf{T^e} \\ \mathbf{P^e} \end{Bmatrix} = \begin{Bmatrix} \mathbf{F_x^e} \\ \mathbf{F_y^e} \\ \mathbf{G^e} \\ \mathbf{0} \end{Bmatrix}, \tag{2.27}$$

where $\mathbf{U^e}$ and $\mathbf{V^e}$ are the nodal dimensionless velocity vectors of the element in the x and y directions respectively; $\mathbf{T^e}$ and $\mathbf{P^e}$ are the nodal dimensionless temperature and pressure vectors of the element; $\mathbf{A_x^e}$, $\mathbf{A_y^e}$, $\mathbf{B_x^e}$, $\mathbf{B_y^e}$ $\mathbf{C_x^e}$, $\mathbf{C_y^e}$, $\mathbf{E^e}$ and $\mathbf{M^e}$ are the property matrices of the element; $\mathbf{F_x^e}$, $\mathbf{F_y^e}$ and $\mathbf{G^e}$ are the dimensionless nodal load vectors due to the dimensionless stress and heat flux on the boundary of the element. These matrices and vectors can be derived and expressed as follows:

$$\mathbf{A}_x^{\mathbf{e}} = \int_A \frac{\partial \boldsymbol{\varphi}}{\partial x^*} K_x^* \boldsymbol{\Psi}^T dA, \qquad \mathbf{B}_x^{\mathbf{e}} = \int_A \boldsymbol{\varphi} K_x^* Ra \boldsymbol{\varphi}^T e_1 dA, \qquad \mathbf{C}_x^{\mathbf{e}} = \int_A \boldsymbol{\Psi} \frac{\partial \boldsymbol{\varphi}^T}{\partial x^*} dA, \tag{2.28}$$

$$\mathbf{A}_y^{\mathbf{e}} = \int_A \frac{\partial \boldsymbol{\varphi}}{\partial y^*} K_y^* \boldsymbol{\Psi}^T dA, \qquad \mathbf{B}_y^{\mathbf{e}} = \int_A \boldsymbol{\varphi} K_y^* Ra \boldsymbol{\varphi}^T e_2 dA, \qquad \mathbf{C}_y^{\mathbf{e}} = \int_A \boldsymbol{\Psi} \frac{\partial \boldsymbol{\varphi}^T}{\partial y^*} dA, \tag{2.29}$$

$$\mathbf{D}_x^{\mathbf{e}}(u^*) = \int_A \boldsymbol{\varphi} u^* \frac{\partial \boldsymbol{\varphi}^T}{\partial x^*} dA, \qquad \mathbf{L}_x^{\mathbf{e}} = \int_A \frac{\partial \boldsymbol{\varphi}}{\partial x^*} \lambda_{ex}^* \frac{\partial \boldsymbol{\varphi}}{\partial x^*} dA, \qquad \mathbf{F}_x^{\mathbf{e}} = \int_S \sigma_x^* \, \boldsymbol{\varphi} dS, \tag{2.30}$$

$$\mathbf{D}_y^{\mathbf{e}}(v^*) = \int_A \boldsymbol{\varphi} v^* \frac{\partial \boldsymbol{\varphi}^T}{\partial x^*} dA, \qquad \mathbf{L}_y^{\mathbf{e}} = \int_A \frac{\partial \boldsymbol{\varphi}}{\partial y^*} \lambda_{ey}^* \frac{\partial \boldsymbol{\varphi}}{\partial y^*} dA, \qquad \mathbf{F}_y^{\mathbf{e}} = \int_S \sigma_y^* \boldsymbol{\varphi} dS, \tag{2.31}$$

$$\mathbf{E}^{\mathbf{e}} = \mathbf{D}_x^{\mathbf{e}}(u^*) + \mathbf{D}_y^{\mathbf{e}}(v^*) + \mathbf{L}_x^{\mathbf{e}} + \mathbf{L}_y^{\mathbf{e}}, \mathbf{G}^{\mathbf{e}} = -\int_S q^* \boldsymbol{\varphi} dS, \tag{2.32}$$

$$\mathbf{M}^{\mathbf{e}} = \int_A \boldsymbol{\varphi} \boldsymbol{\varphi}^T dA, \qquad q^* = \frac{H}{\Delta T \lambda_{e0}} q, \qquad \sigma^* = \frac{K_h \rho_{f0} c_p}{\mu \lambda_{e0}} \sigma, \tag{2.33}$$

where $\boldsymbol{\varphi}$ is the shape function vector for the temperature and velocity components of the element; $\boldsymbol{\Psi}$ is the shape function vector for the pressure of the element; σ and q are the stress and heat flux on the boundary of the element; A and S are the area and boundary length of the element.

It is noted that since the full nonlinear term of the energy equation in the Horton-Rogers-Lapwood problem is considered in the finite element analysis, matrix $\mathbf{E}^{\mathbf{e}}$ is dependent on the velocity components of the element. Thus, a prediction for the initial velocities of an element is needed to have this matrix evaluated. This is the main motivation for proposing a progressive asymptotic approach procedure in the next section.

From the penalty finite element approach (Zienkiewicz 1977), the following equation exists:

$$\mathbf{C}_{\mathbf{x}}^{\mathbf{e}} \mathbf{U}^{\mathbf{e}} + \mathbf{C}_{\mathbf{y}}^{\mathbf{e}} \mathbf{V}^{\mathbf{e}} = -\varepsilon \mathbf{M}_{\mathbf{p}} \mathbf{P}^{\mathbf{e}}. \tag{2.34}$$

Equation (2.34) can be rewritten as

$$\mathbf{P}^{\mathbf{e}} = -\frac{1}{\varepsilon} \mathbf{M}_{\mathbf{p}}^{-1} (\mathbf{C}_{\mathbf{x}}^{\mathbf{e}} \mathbf{U}^{\mathbf{e}} + \mathbf{C}_{\mathbf{y}}^{\mathbf{e}} \mathbf{V}^{\mathbf{e}}). \tag{2.35}$$

Substituting Eq. (2.35) into Eq. (2.27) yields the following equation in the elemental level:

$$\begin{bmatrix} \mathbf{Q}^{\mathbf{e}} & -\mathbf{B}^{\mathbf{e}} \\ \mathbf{0} & \mathbf{E}^{\mathbf{e}} \end{bmatrix} \begin{Bmatrix} \mathbf{U}_{\mathbf{F}}^{\mathbf{e}} \\ \mathbf{T}^{\mathbf{e}} \end{Bmatrix} = \begin{Bmatrix} \mathbf{F}^{\mathbf{e}} \\ \mathbf{G}^{\mathbf{e}} \end{Bmatrix}, \tag{2.36}$$

where

$$\mathbf{Q}^{\mathbf{e}} = \overline{\mathbf{M}}^{\mathbf{e}} + \frac{1}{\varepsilon} \mathbf{A}^{\mathbf{e}} (\mathbf{M}_{\mathbf{p}}^{\mathbf{e}})^{-1} (\mathbf{C}^{\mathbf{e}})^T, \tag{2.37}$$

$$\overline{\mathbf{M}}^{\mathbf{e}} = \begin{bmatrix} \mathbf{M}^{\mathbf{e}} & \mathbf{0} \\ \mathbf{0} & \mathbf{M}^{\mathbf{e}} \end{bmatrix}, \qquad \mathbf{U}_{\mathrm{F}}^{\mathbf{e}} = \begin{Bmatrix} \mathbf{U}^{\mathbf{e}} \\ \mathbf{V}^{\mathbf{e}} \end{Bmatrix}, \qquad \mathbf{F}^{\mathbf{e}} = \begin{Bmatrix} \mathbf{F}_x^{\mathbf{e}} \\ \mathbf{F}_y^{\mathbf{e}} \end{Bmatrix}, \tag{2.38}$$

$$\mathbf{B}^{\mathbf{e}} = \begin{Bmatrix} \mathbf{B}_x^{\mathbf{e}} \\ \mathbf{B}_y^{\mathbf{e}} \end{Bmatrix}, \qquad \mathbf{A}^{\mathbf{e}} = \begin{Bmatrix} \mathbf{A}_x^{\mathbf{e}} \\ \mathbf{A}_y^{\mathbf{e}} \end{Bmatrix}, \qquad \mathbf{C}^{\mathbf{e}} = \begin{Bmatrix} \mathbf{C}_x^{\mathbf{e}} \\ \mathbf{C}_y^{\mathbf{e}} \end{Bmatrix}, \tag{2.39}$$

$$\mathbf{M}_{\mathbf{p}}^{\mathbf{e}} = \int_A \boldsymbol{\Psi}\boldsymbol{\Psi}^T dA. \tag{2.40}$$

It needs to be pointed out that ε is a penalty parameter in Eq. (2.37). For the purpose of obtaining an accurate solution, this parameter must be chosen small enough to approximate fluid incompressibility well, but large enough to prevent the resulting matrix problem from becoming too ill-conditioned to solve.

By assembling all elements in a system, the finite element equation of the system can be expressed in a matrix form as

$$\begin{bmatrix} \mathbf{Q} & -\mathbf{B} \\ \mathbf{0} & \mathbf{E}(\mathbf{U}) \end{bmatrix} \begin{Bmatrix} \mathbf{U_F} \\ \mathbf{T} \end{Bmatrix} = \begin{Bmatrix} \mathbf{F} \\ \mathbf{G} \end{Bmatrix}, \tag{2.41}$$

where **Q**, **B** and **E** are global property matrices of the system; $\mathbf{U_F}$ and **T** are global nodal velocity and temperature vectors of the system; **F** and **G** are global nodal load vectors of the system. Since Equation (2.41) is nonlinear, either the successive substitution method or the Newton-Raphson method can be used to solve this equation.

2.3 The Progressive Asymptotic Approach Procedure for Solving Steady-State Natural Convection Problems in Fluid-Saturated Porous Media

To solve the steady-state Horton-Rogers-Lapwood problem with the full nonlinear term of the energy equation included in the finite element analysis, the asymptotic approach concept (Cook et al. 1989, Zhao and Steven 1996a, b, c) needs to be used in a progressive fashion (Zhao et al. 1997a). If the gravity acceleration is assumed to tilt at a small angle, α, in the Horton -Rogers-Lapwood problem, then a non-zero velocity field in a fluid-saturated porous medium may be found using the finite element method. The resulting non-zero velocity field can be used as the initial velocity field of the pore-fluid to solve the original Horton-Rogers-Lapwood problem with the tilted small angle being zero. Thus, two kinds of problems need to be progressively solved in the finite element analysis. One is the modified Horton-Rogers-Lapwood problem, in which the gravity acceleration is tilted a small angle, and another is the original Horton-Rogers-Lapwood problem. This forms two basic steps of the progressive asymptotic approach procedure. Clearly, the basic idea behind the progressive asymptotic approach procedure is that when the small angle tilted by the gravity acceleration approaches zero, the modified Horton-Rogers-Lapwood problem asymptotically approaches the original one and as a result, a solution to the original Horton-Rogers-Lapwood problem can be obtained.

Based on the basic idea behind the progressive asymptotic approach procedure, the key issue of obtaining a non-zero pore-fluid flow solution for the Horton-Rogers-Lapwood problem is to choose the initial velocity field of pore-fluid correctly. If the initial velocity field is not correctly chosen, the finite element method will lead to

a zero pore-fluid flow solution for natural convection of pore-fluid, even though the Rayleigh number is high enough to drive the occurrence of natural convection in a fluid-saturated porous medium. In order to overcome this difficulty, a modified Horton-Rogers-Lapwood problem, in which the gravity acceleration is assumed to tilt a small angle α, needs to be solved. Supposing the original Horton-Rogers-Lapwood problem has a Rayleigh number (Ra) and that the non-zero solution for the modified Horton-Rogers-Lapwood problem is $S(Ra, \alpha)$, it is possible to find a non-zero solution for the original Horton-Rogers-Lapwood problem by taking a limit of $S(Ra, \alpha)$ when α approaches zero. This process can be mathematically expressed as follows:

$$\lim_{\alpha \to 0} S(Ra,\ \alpha) = S(Ra,\ 0), \tag{2.42}$$

where $S(Ra,\ 0)$ is a solution for the original Horton-Rogers-Lapwood problem; $S(Ra,\ \alpha)$ is the solution for the modified Horton-Rogers-Lapwood problem; S is any variable to be solved in the original Horton-Rogers-Lapwood problem.

It is noted that in theory, if $S(Ra,\ \alpha)$ could be expressed as a function of α explicitly, $S(Ra,\ 0)$ would follow immediately. However, in practice, it is necessary to find out $S(Ra,\ 0)$ numerically since it is very difficult and often impossible to express $S(Ra,\ \alpha)$ in an explicit manner. Thus, the question which must be answered is how to choose α so as to obtain an accurate non-zero solution, $S(Ra,\ 0)$. From the theoretical point of view, it is desirable to choose α as small as possible. The reason for this is that the smaller the value of α, the closer the characteristic of $S(Ra,\ \alpha)$ to that of $S(Ra,\ 0)$. This enables a more accurate solution $S(Ra,\ 0)$ to be obtained in the computation. From the finite element analysis point of view, α cannot be chosen too small because the smaller the value of α, the more sensitive the solution $S(Ra,\ \alpha)$ to the initial velocity field of pore-fluid. As a result, a very small α usually leads to a zero velocity field due to any inappropriate choice for the initial velocity field of pore-fluid. To avoid this phenomenon, α should be chosen big enough to eliminate the strong dependence of $S(Ra,\ \alpha)$ on the initial velocity field of pore-fluid. For the purpose of using a big value of α and keeping the final solution $S(Ra,\ 0)$ of good accuracy in the finite element analysis, $S(Ra,\ \alpha)$ needs to approach $S(Ra,\ 0)$ in a progressive asymptotic manner, as clearly shown in Fig. 2.1. This leads to the following processes mathematically:

$$\lim_{\alpha_i \to \alpha_{i+1}} S(Ra,\ \alpha_i) = S(Ra,\ \alpha_{i+1}) \qquad (i = 1, 2, ..., n-1), \tag{2.43}$$

$$\lim_{\alpha_n \to 0} S(Ra,\ \alpha_n) = S(Ra,\ 0), \tag{2.44}$$

$$\alpha_1 = \alpha, \qquad \alpha_{i+1} = \frac{1}{R}\alpha_i, \tag{2.45}$$

where n is the total step number for α approaching zero; R is the rate of α_i approaching α_{i+1}. Generally, the values of α,n and R are dependent on the nature of a problem to be analysed.

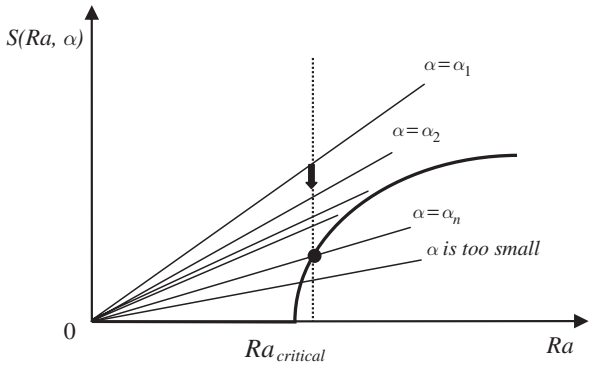

Fig. 2.1 The basic concept of the progressive asymptotic approach procedure

For solving the steady-state Horton-Rogers-Lapwood problem using the progressive asymptotic approach procedure associated with the finite element method, numerical experience has shown that $1^\circ \leq \alpha \leq 5^\circ$, $5 \leq R \leq 10$ and $1 \leq n \leq 2$ leads to acceptable solutions. Therefore, for α in the range of 1–5° and R in the range of 5–10, $S(Ra, \alpha)$ can asymptotically approach $S(Ra, 0)$ in one step or two steps. This indicates the efficiency of the present procedure.

2.4 Derivation of Analytical Solution to a Benchmark Problem

In order to verify the applicability of the progressive asymptotic approach procedure for solving the Horton-Rogers-Lapwood convection problem, an analytical solution is needed for a benchmark problem, the geometry and boundary conditions of which can be exactly modelled by the finite element method. Although the existing solutions (Phillips 1991, Nield and Bejan 1992) for a horizontal layer in porous media can be used to check the accuracy of a finite element solution within a square box with appropriate boundary conditions, it is highly desirable to examine the progressive asymptotic approach procedure as extensively as possible. For this purpose, a benchmark problem of any rectangular geometry is constructed and shown in Fig. 2.2. Without losing generality, the dimensionless governing equations given in Eqs. (2.10), (2.11), (2.12) and (2.13) are considered in this section. The boundary conditions of the benchmark problem are expressed using the dimensionless variables as follows:

$$u^* = 0, \qquad \frac{\partial T^*}{\partial x^*} = 0 \qquad (\text{at } x^* = 0 \text{ and } x^* = L^*), \tag{2.46}$$

$$v^* = 0, \qquad T^* = 1 \qquad (\text{at } y^* = 0), \tag{2.47}$$

$$v^* = 0, \qquad T^* = 0 \qquad (\text{at } y^* = 1), \tag{2.48}$$

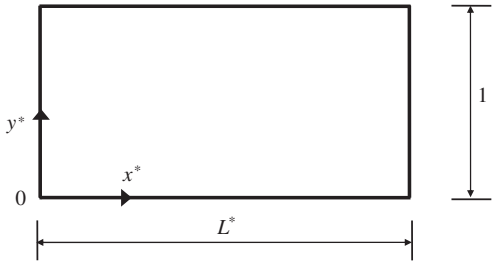

Fig. 2.2 Geometry of a benchmark problem

where L^* is a dimensionless length in the horizontal direction and $L^* = L/H$, in which L is the real length of the problem domain in the horizontal direction.

For ease of deriving an analytical solution to the benchmark problem, it is assumed that the porous medium under consideration is fluid-saturated and isotropic. This means that $K_x = K_y = K_h$ and $\lambda_{ex} = \lambda_{ey} = \lambda_{e0}$. As a result, Eqs. (2.10), (2.11), (2.12) and (2.13) can be further simplified as follows:

$$\frac{\partial u^*}{\partial x^*} + \frac{\partial v^*}{\partial y^*} = 0, \tag{2.49}$$

$$u^* = -\frac{\partial P^*}{\partial x^*} + RaT^* e_1, \tag{2.50}$$

$$v^* = -\frac{\partial P^*}{\partial y^*} + RaT^* e_2, \tag{2.51}$$

$$u^* \frac{\partial T^*}{\partial x^*} + v^* \frac{\partial T^*}{\partial y^*} = \frac{\partial^2 T^*}{\partial x^{*2}} + \frac{\partial^2 T^*}{\partial y^{*2}}. \tag{2.52}$$

Using the linearization procedure for temperature gradient and a dimensionless stream function Ψ simultaneously, Eqs. (2.49), (2.50), (2.51) and (2.52) are reduced to the following two equations:

$$\frac{\partial^2 \Psi}{\partial x^{*2}} + \frac{\partial^2 \Psi}{\partial y^{*2}} = -Ra \frac{\partial T^*}{\partial x^*}, \tag{2.53}$$

$$\frac{\partial \Psi}{\partial x^*} = \frac{\partial^2 T^*}{\partial x^{*2}} + \frac{\partial^2 T^*}{\partial y^{*2}}. \tag{2.54}$$

Since Eqs. (2.53) and (2.54) are linear, solutions to Ψ and T^* are of the following forms:

$$\Psi = f(y^*) \sin\left(q \frac{x^*}{L^*}\right) \qquad (q = m\pi, m = 1, 2, 3, ...), \tag{2.55}$$

$$T^* = \theta(y^*)\cos\left(q\frac{x^*}{L^*}\right) + (1 - y^*) \qquad (q = m\pi, m = 1, 2, 3, ...). \tag{2.56}$$

Substituting Eqs. (2.55) and (2.56) into Eqs. (2.53) and (2.54) yields the following equations:

$$f''(y^*) - \left(\frac{q}{L^*}\right)^2 f(y^*) = \frac{q}{L^*} Ra\theta(y^*), \tag{2.57}$$

$$\frac{q}{L^*} f(y^*) = -\left(\frac{q}{L^*}\right)^2 \theta(y^*) + \theta''(y^*). \tag{2.58}$$

Combining Eqs. (2.57) and (2.58) leads to an equation containing $f(y^*)$ only:

$$f^{IV}(y^*) - 2\left(\frac{q}{L^*}\right)^2 f''(y^*) - \left(\frac{q}{L^*}\right)^2 \left[Ra - \left(\frac{q}{L^*}\right)^2\right] f(y^*) = 0. \tag{2.59}$$

It is immediately noted that Equation (2.59) is a linear, homogeneous ordinary differential equation so that it has a zero trivial solution. For the purpose of finding out a non-zero solution, it is noted that the non-zero solution satisfying both Equation (2.59) and the boundary conditions in Eqs. (2.46), (2.47) and (2.48) can be expressed as

$$f(y^*) = \sin(ry^*) \qquad (r = n\pi, n = 1, 2, 3, ...). \tag{2.60}$$

Using this equation, the condition under which the non-zero solution exists for Eq. (2.59) is derived and expressed as

$$Ra = \left(\frac{L^*}{q}r^2 + \frac{q}{L^*}\right)^2 = \left(\frac{n^2}{m}L^* + \frac{m}{L^*}\right)^2 \pi^2 \tag{2.61}$$
$$(m = 1, 2, 3, ..., n = 1, 2, 3, ...).$$

It can be observed from Eq. (2.61) that in the case of L^* being an integer, the minimum Rayleigh number is $4\pi^2$, which occurs when n = 1 and $m = L^*$. However, if L^* is not an integer, the minimum Rayleigh number is $(L^* + 1/L^*)^2\pi^2$, which occurs when $m = 1$ and $n = 1$. Since the minimum Rayleigh number determines the onset of natural convection in a fluid-saturated porous medium for the Horton-Rogers-Lapwood problem, it is often labelled as the critical Rayleigh number, $Ra_{critical}$.

For this benchmark problem, the mode shapes for the stream function and related dimensionless variables corresponding to the critical Rayleigh number can be derived and expressed as follows:

$$\Psi = C_1 \sin\left(\frac{m\pi}{L^*}x^*\right)\sin(n\pi y^*), \tag{2.62}$$

$$u^* = n\pi C_1 \sin\left(\frac{m\pi}{L^*}x^*\right)\cos(n\pi y^*), \tag{2.63}$$

$$v^* = -\frac{m\pi}{L^*}C_1 \cos\left(\frac{m\pi}{L^*}x^*\right)\sin(n\pi y^*), \tag{2.64}$$

$$T^* = -\frac{C_1}{\sqrt{Ra_{critical}}}\cos\left(\frac{m\pi}{L^*}x^*\right)\sin(n\pi y^*) + (1 - y^*), \tag{2.65}$$

$$P^* = \frac{nL^*}{m}C_1 \cos\left(\frac{m\pi}{L^*}x^*\right)\cos(n\pi y^*) - \frac{Ra_{critical}}{2}(1 - y^*)^2 + C_2, \tag{2.66}$$

where the values of m, n and $Ra_{critical}$ are dependent on whether L^* is an integer or not; C_1 is a non-zero constant and C_2 is an arbitrary constant. It is interesting to note that since $Ra_{critical}$ is a function of L^*, it can vary with a non-integer L^*. This implies that if rectangular valleys are filled with porous media, they may have different critical Rayleigh numbers when their ratios of length to height are different.

2.5 Verification of the Proposed Progressive Asymptotic Approach Procedure Associated with Finite Element Analysis

Using the analytical solution derived for a benchmark problem in the last section, the proposed progressive asymptotic approach procedure associated with the finite element analysis for solving the Horton-Rogers-Lapwood problem in a fluid-saturated porous medium is verified in this section. A rectangular domain of $L^* = 1.5$ is considered in the calculation. The critical Rayleigh number for the test problem considered is $169\pi^2/36$. As shown in Fig. 2.3, the problem domain is discretized into

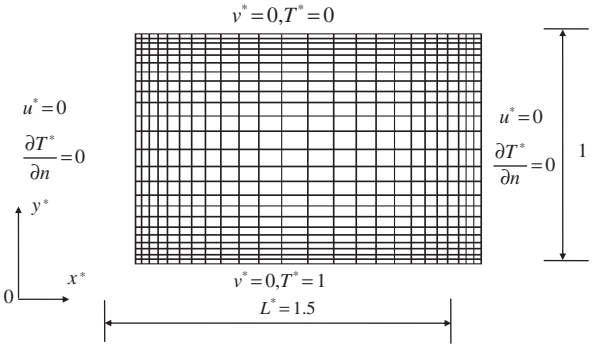

Fig. 2.3 Finite element mesh for the benchmark problem

864 nine-node quadrilateral elements of 3577 nodes in total. The mesh gradation technique, which enables the region in the vicinity of problem boundaries to be modelled using finite elements of small sizes, has been employed to increase the solution accuracy in this region. The following parameters associated with the progressive asymptotic approach procedure are used in the calculation: $\alpha = 5^o$, $n = 2$ and $R = 5$.

Figures 2.4, 2.5, 2.6 and 2.7 show the comparison of numerical solutions with analytical ones for dimensionless velocity, stream function, temperature and pressure modes respectively. In these figures, the plots above are analytical solutions, whereas the plots below are numerical solutions for the problem. It is observed from these results that the numerical solutions from the progressive asymptotic approach procedure associated with the finite element method are in good agreement with the analytical solutions. Compared with the analytical solutions, the maximum error in the numerical solutions is less than 2%. This demonstrates the usefulness of the present progressive asymptotic approach procedure when it is used to solve the steady-state Horton-Rogers-Lapwood problems.

At this point, there is a need to explain why both the analytical and the numerical solutions for the pore-fluid flow are non-symmetric, although the geometry and boundary conditions for the problem are symmetric. As stated previously, the Horton-Rogers-Lapwood problem belongs mathematically to a bifurcation problem. The trivial solution for the pore-fluid flow of the problem is zero. That is to say, if the Rayleigh number of the problem is less than the critical Rayleigh number, the solution resulting from any small disturbance or perturbation converges to the trivial

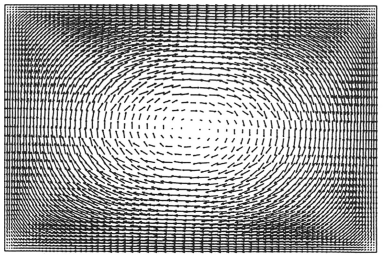

(Analytical solution)

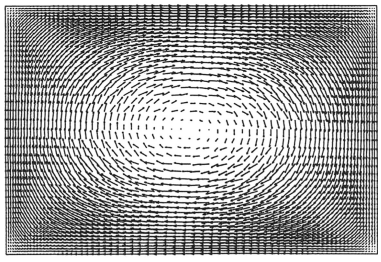

(Numerical solution)

Fig. 2.4 Comparison of numerical solution with analytical solution (Dimensionless velocity)

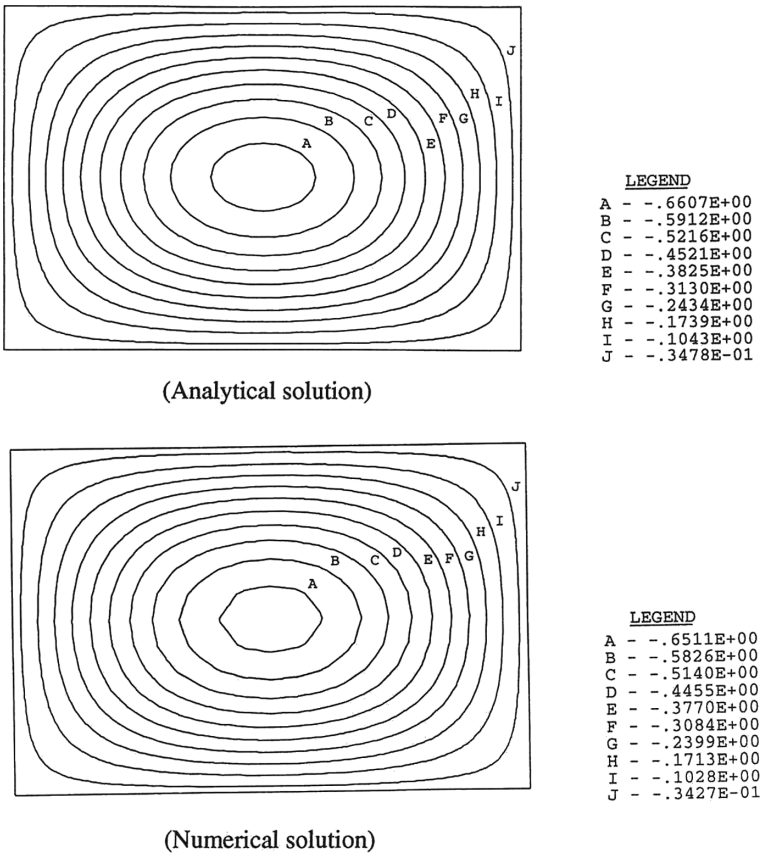

Fig. 2.5 Comparison of numerical solution with analytical solution (Dimensionless stream function)

solution. In this case, the solution for the pore-fluid flow is zero (and, of course, symmetric) and the system is in a stable state. However, if the Rayleigh number of the problem is equal to or greater than the critical Rayleigh number, the solution resulting from any small disturbance or perturbation may lead to a non-trivial solution. In this situation, the solution for the pore-fluid flow is non-zero and the system is in an unstable state. Since the main purpose of this study is to find out the non-trivial solution for problems having a high Rayleigh number, $Ra \geq Ra_{critical}$, a small disturbance or perturbation needs to be applied to the system at the beginning of a computation. This is why gravity is firstly tilted a small angle away from vertical and then gradually approaches and is finally restored to vertical in the proposed progressive asymptotic approach procedure. It is the small perturbation that makes the non-trivial solution non-symmetric, even though the system considered is symmetric. In addition, as addressed in Sect. 2.3, the solution dependence on the amplitude of the initially-tilted small angle can be avoided by making this angle approach zero

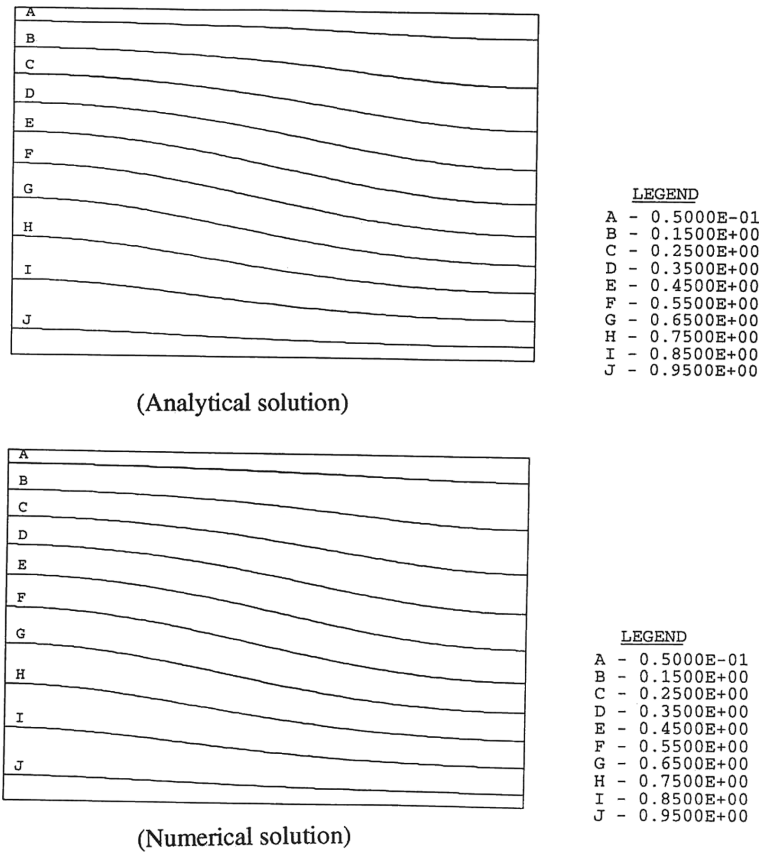

Fig. 2.6 Comparison of numerical solution with analytical solution (Dimensionless temperature)

in a progressive asymptotic manner. However, since there are two possible non-symmetric solutions for convective pore-fluid flow, namely a clockwise convective flow and an anti-clockwise convective flow, the solution dependence on the direction of the initially-tilted small angle cannot be avoided.

2.6 Application of the Progressive Asymptotic Approach Procedure Associated with Finite Element Analysis

2.6.1 Two-Dimensional Convective Pore-Fluid Flow Problems

The present progressive asymptotic approach procedure is employed to investigate the effect of basin shapes on natural convection in a fluid-saturated porous medium when it is heated from below. Three different basin shapes having square,

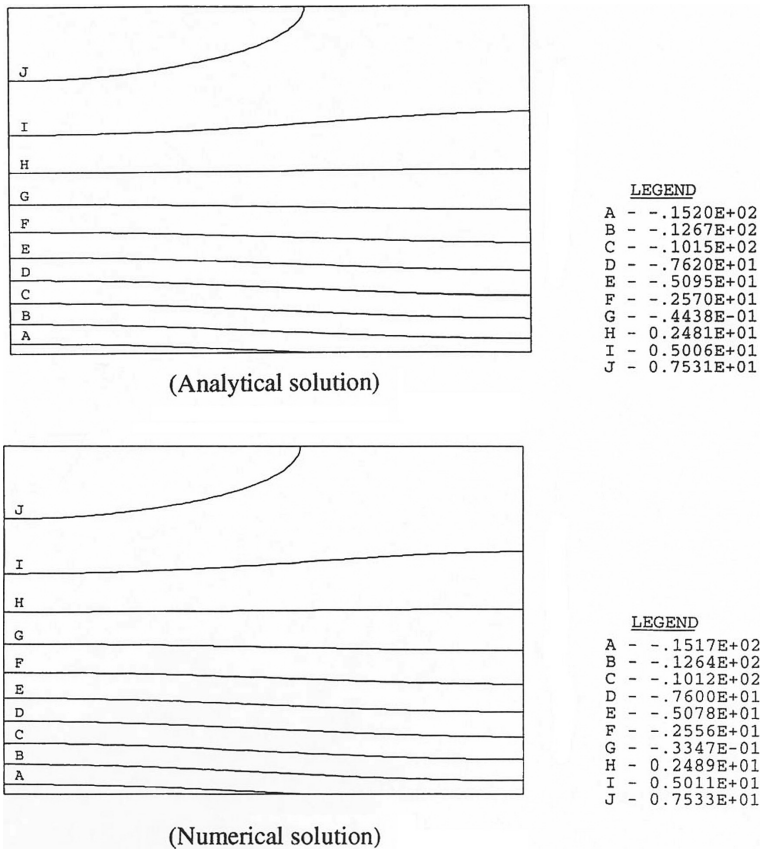

Fig. 2.7 Comparison of numerical solution with analytical solution (Dimensionless pressure)

rectangular and trapezoidal geometries, which are filled with fluid-saturated porous media, are considered in the analysis. For the rectangular basin, the ratio of width to height is 1.5. For the trapezoidal basin, the ratios of top width to height and bottom width to height are 2 and 1 respectively. In order to reflect the anisotropic behaviour of the porous media, the medium permeability in the horizontal direction is assumed to be three times that in the vertical direction. As shown in Fig. 2.8, all three basins are discretized into 484 nine-node quadrilateral elements of 2041 nodes in total. The boundary conditions of the problems are also shown in Fig. 2.8, in which n is the normal direction of a boundary. Two Rayleigh numbers, namely $Ra = 80$ and $Ra = 400$, are used to examine the effect of the Rayleigh number on natural convection in a fluid-saturated porous medium. The same parameters as used in the above model verification examples have been used here for the progressive asymptotic approach procedure.

Figure 2.9 shows the dimensionless velocity distribution for the three different basins, whereas Figs. 2.10 and 2.11 show the dimensionless streamline contours

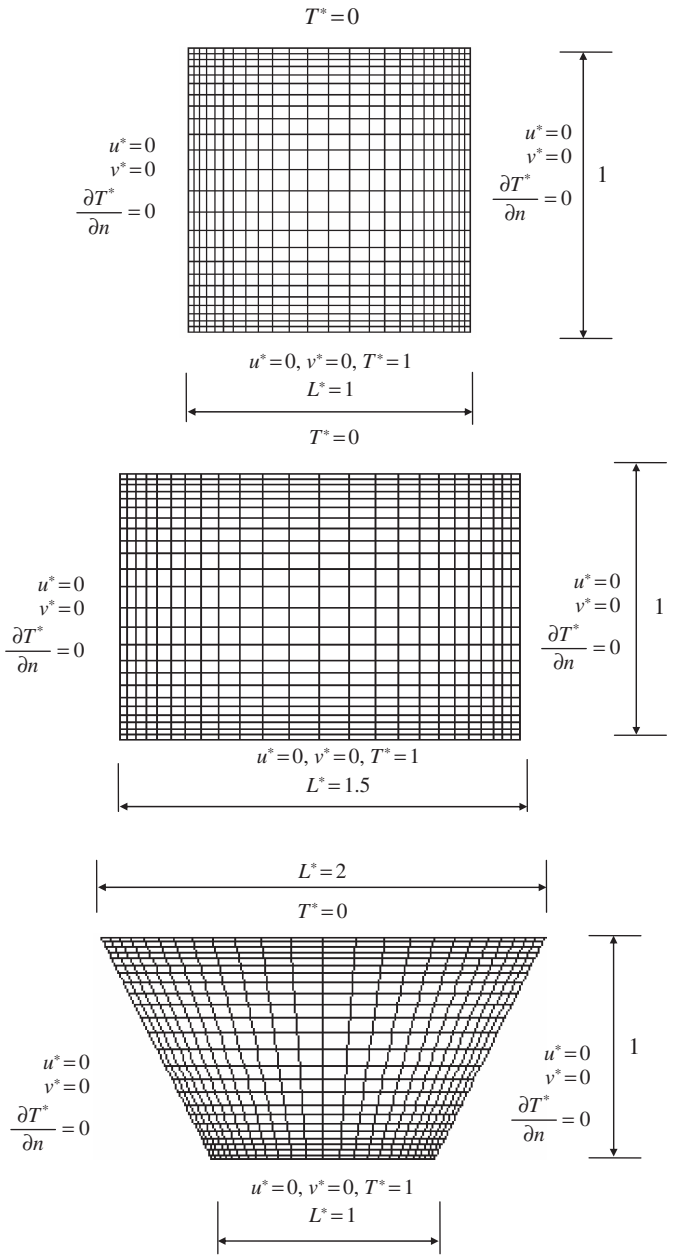

Fig. 2.8 Finite element meshes for three different basins shapes

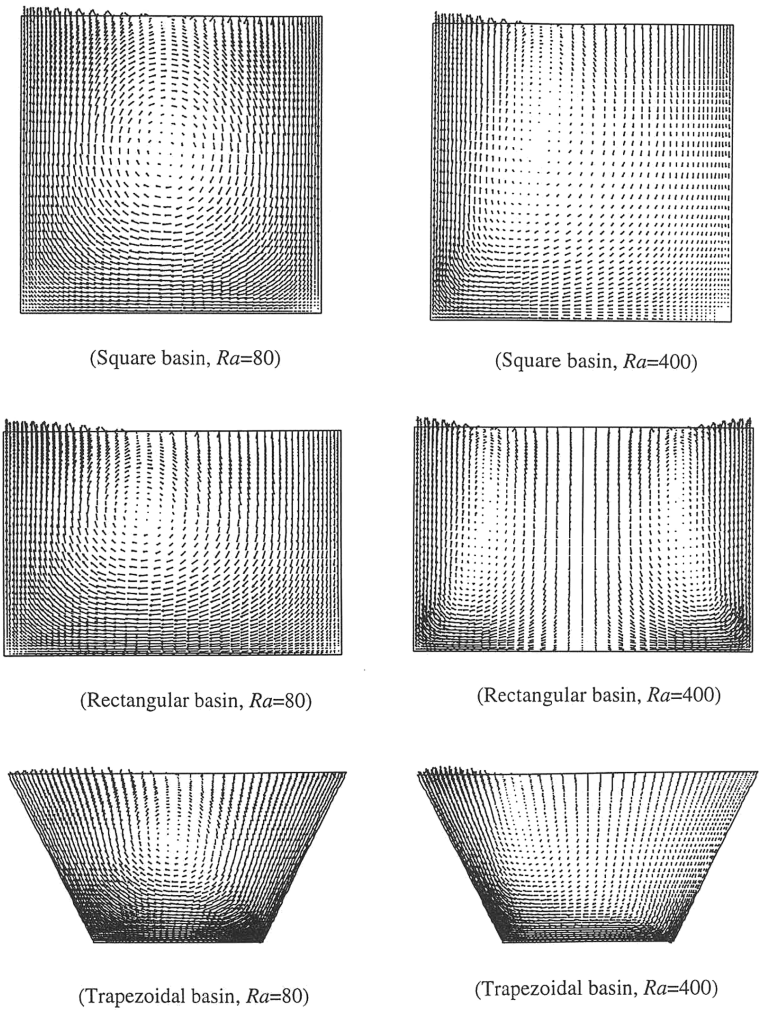

Fig. 2.9 Dimensionless velocity distribution for different basins

due to different basin shapes for $Ra = 80$ and $Ra = 400$ respectively. It is obvious that different basin shapes have a considerable effect on the patterns of convective flow in the fluid-saturated porous medium, especially in the case of higher Rayleigh numbers. Apart from notable differences in velocity distribution patterns, maximum velocity amplitudes for three different basins are also significantly different. For instance, in the case of $Ra = 80$, the maximum amplitudes of dimensionless velocities are 5.29, 8.93 and 11.66 for square, rectangular and trapezoidal basins respectively. This fact indicates that different basin shapes may affect the contaminant transport or mineralization processes in a fluid-saturated porous medium once natural convection is initiated in the medium.

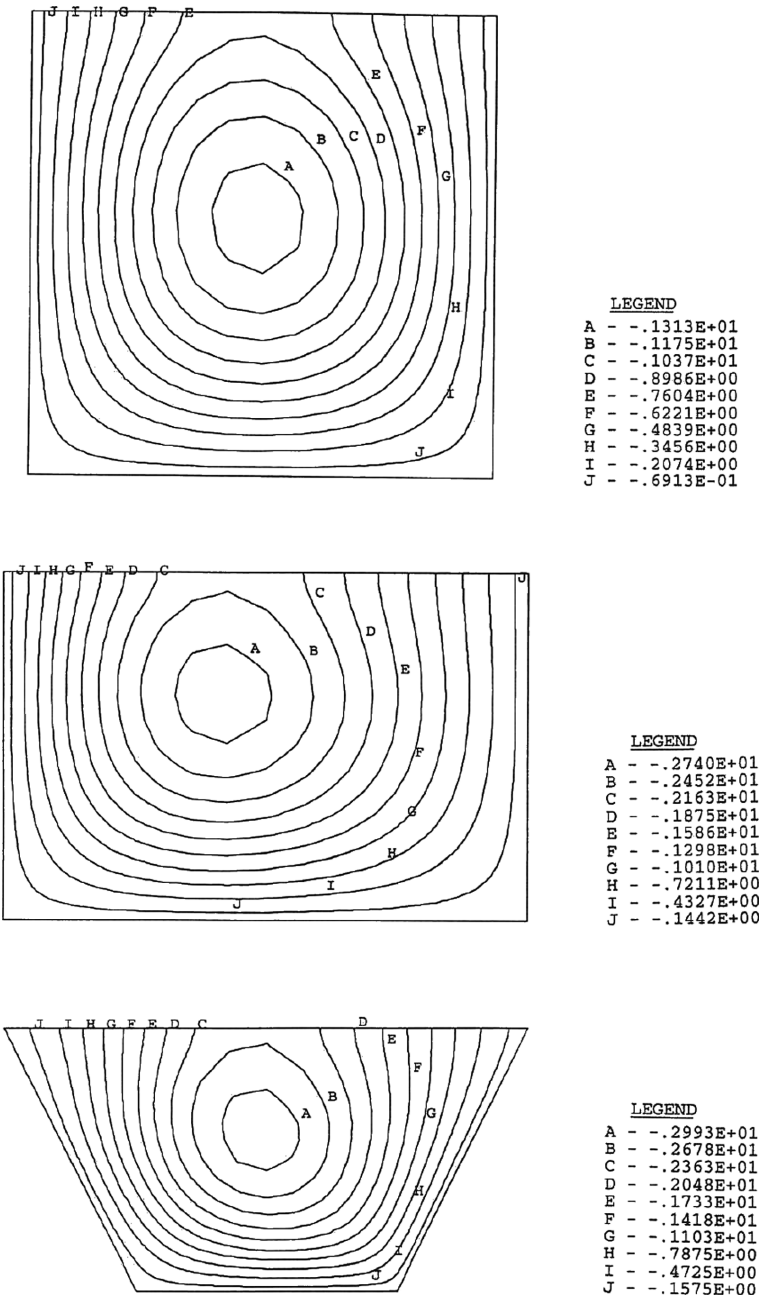

Fig. 2.10 Dimensionless streamline contours for different basins ($Ra = 80$)

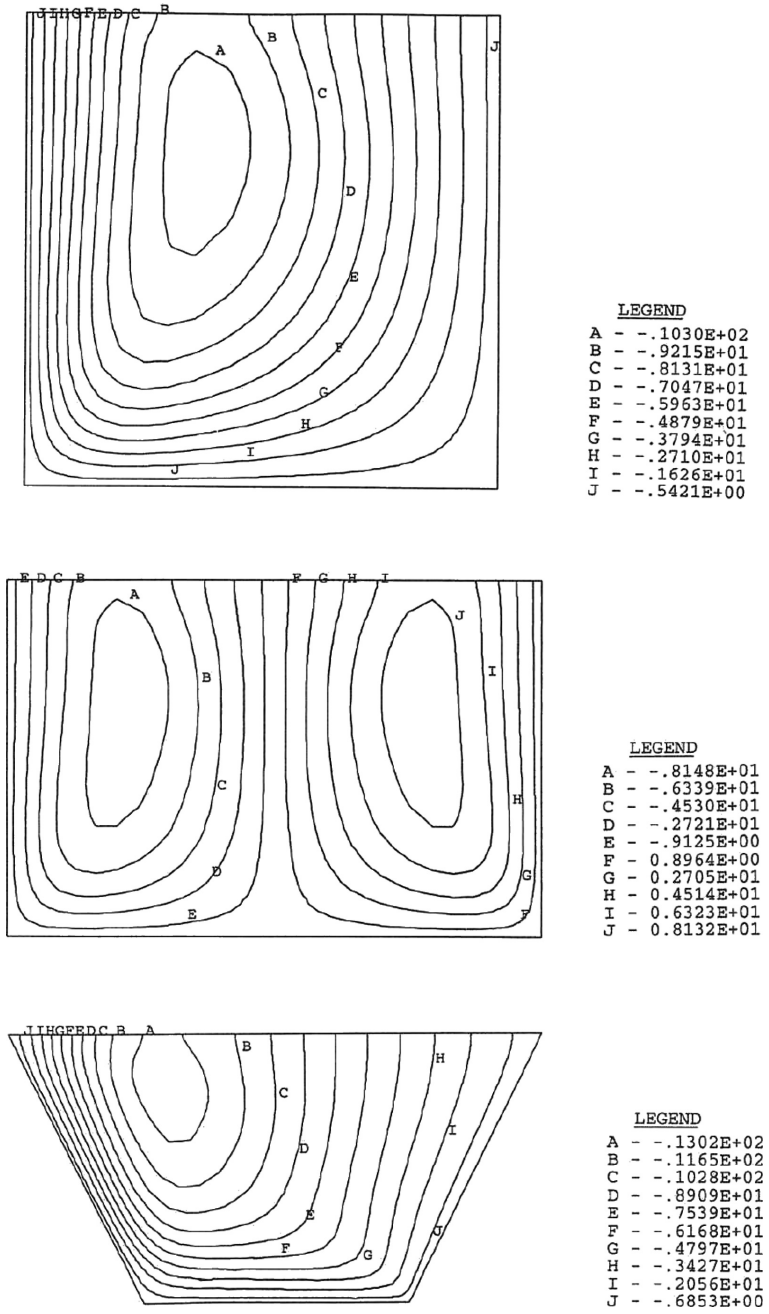

Fig. 2.11 Dimensionless streamline contours for different basins ($Ra = 400$)

2.6.2 Three-Dimensional Convective Pore-Fluid Flow Problems

The proposed progressive asymptotic approach procedure can be straightforwardly extended to the simulation of three-dimensional convective pore-fluid flow problems in fluid-saturated porous media (Zhao et al. 2001a, 2003a). Since the streamline function is not available for three dimensional fluid flow problems, it is necessary to use the particle tracking technique to show particle movements in three dimensional fluid flow systems. In the particle tracking technique, a fundamental problem, which needs to be solved effectively, is as follows. If the initial (known) location of a particle is point A (x_A, y_A, z_A), where x_A, y_A and z_A are the coordinate components of point A in the x, y and z directions of a global coordinate system, then we need to determine where the new location (i.e. point A') of this particle is after a given time interval, Δt. Clearly, if the velocity of the particle at point A is known, then the coordinate components of point A' in the global coordinate system can be approximately determined for a small Δt as follows:

$$x_{A'} = x_A + u_A \Delta t, \tag{2.67}$$

$$y_{A'} = y_A + v_A \Delta t, \tag{2.68}$$

$$z_{A'} = z_A + w_A \Delta t, \tag{2.69}$$

where $x_{A'}$, $y_{A'}$ and $z_{A'}$ are the coordinate components of point A' in the x, y and z directions of the global coordinate system; u_A, v_A and w_A are the velocity components of point A in the x, y and z directions of the global coordinate system, respectively.

In general cases, the location of point A is not coincident with the nodal points in a finite element analysis so that the consistent interpolation of the finite element solution is needed to determine the velocity components at this point. For this purpose, it is essential to find the coordinate components of point A in the local coordinate system from the following equations for an isoparametric finite element.

$$x_A = \sum_{i=1}^{n} \phi_i(\xi_A, \eta_A, \zeta_A) x_i, \tag{2.70}$$

$$y_A = \sum_{i=1}^{n} \phi_i(\xi_A, \eta_A, \zeta_A) y_i, \tag{2.71}$$

$$z_A = \sum_{i=1}^{n} \phi_i(\xi_A, \eta_A, \zeta_A) z_i, \tag{2.72}$$

where x_A, y_A and z_A are the coordinate components of point A in the x, y and z directions of the global coordinate system; ξ_A, η_A and ζ_A are three coordinate components

of point A in the ξ, η and ζ directions of a local coordinate system; x_i, y_i and z_i are the coordinate components of nodal point i in the x, y and z directions of the global coordinate system; n is the total nodal number of the element containing point A; ϕ_i is the interpolation function of node i in the element containing point A.

In Eqs. (2.70), (2.71) and (2.72), the coordinate components of point A in the global coordinate system are known, so that the coordinate components of this point in the local system can be determined using any inverse mapping technique (Zhao et al. 1999f). Once the coordinate components of point A in the global coordinate system are determined, the velocity components of point A in the global system can be straightforwardly calculated as follows:

$$u_A = \sum_{i=1}^{n} \phi_i(\xi_A,\ \eta_A,\ \zeta_A)u_i \tag{2.73}$$

$$v_A = \sum_{i=1}^{n} \phi_i(\xi_A,\ \eta_A,\ \zeta_A)v_i \tag{2.74}$$

$$w_A = \sum_{i=1}^{n} \phi_i(\xi_A,\ \eta_A,\ \zeta_A)w_i, \tag{2.75}$$

where u_A, v_A and w_A are the velocity components of point A in the x, y and z directions of the global coordinate system; u_i, v_i and w_i are the velocity components of nodal point i in the x, y and z directions of the global coordinate system, respectively.

The above-mentioned process indicates that in the finite element analysis of fluid flow problems, the trajectory of any given particle can be calculated using the nodal coordinate and velocity components, which are fundamental quantities and therefore available in the finite element analysis.

To demonstrate the applicability of the progressive asymptotic approach procedure for simulating convective pore-fluid flow in three dimensional situations, the example considered in this section is a cubic box of $10 \times 10 \times 10\,km^3$ in size. This box is filled with pore-fluid saturated porous rock, which is a part of the upper crust of the Earth. In order to simulate geothermal conditions in geology, the bottom of the box is assumed to be hotter than the top of the box. This means that the pore-fluid saturated porous rock is uniformly heated from below. For the system considered here, the classical analysis (Phillips 1991, Nield and Bejan 1992, Zhao et al. 1997a) indicates that the convective flow is possible when the Rayleigh number of the system is either critical or supercritical. For this reason, the parameters and properties of the system are deliberately selected in such a way that the Rayleigh number of the system is supercritical.

Figure 2.12 shows the finite element mesh of 8000 cubic elements for the three dimensional convective flow problem. For the purpose of investigating the perturbation direction on the pattern of convective flow, two cases are considered in the following computations. In the first case, the perturbation of gravity is applied in the x-z plane only. This means that the problem is axisymmetrical about the y axis so that

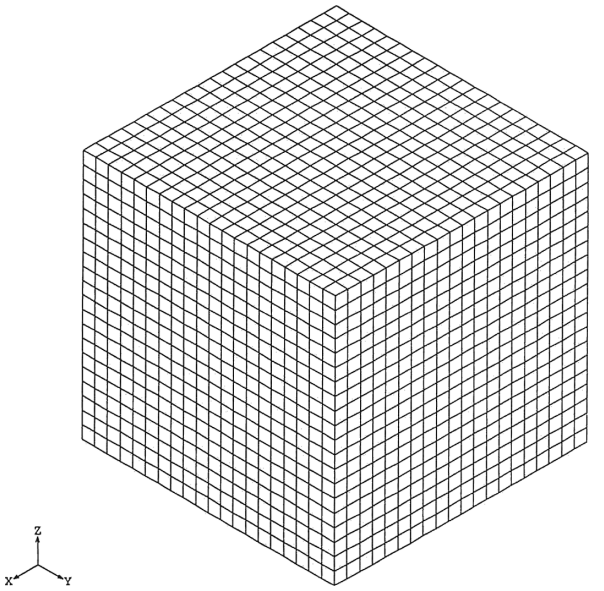

Fig. 2.12 Finite element mesh for the three-dimensional problem

the problem can be degenerated into a two dimensional problem, from the mathematical and analytical points of view. Since the solutions for the axisymmetrical convective flow problem are available (Nield and Bejan 1992, Zhao et al. 1997a), the numerical methods used in this study can be verified by comparing the related analytical solutions with the solutions obtained from this special three dimensional case (i.e. axisymmetrical case). In the second case, the perturbation of gravity is equally applied in both the *x*-*z* and *y*-*z* planes. This means that a true three dimensional convective flow problem is considered in this case. Table 2.1 shows the parameters used in the computations for both cases. To reflect the three-dimensional features of convective pore-fluid flow, the following boundary conditions are used. Temperatures at

Table 2. 1 Parameters used for the three-dimensional convective flow problem

Material type	Parameter	Value
pore-fluid	dynamic viscosity	$10^{-3}\,\mathrm{N}\times\mathrm{s/m^2}$
	reference density	$1000\,\mathrm{kg/m^3}$
	volumetric thermal expansion coefficient	$2.07\times10^{-4}\,1/^{\circ}\mathrm{C}$
	specific heat	$4185\,\mathrm{J/(kg\times{}^0C)}$
	thermal conductivity coefficient	$0.6\,\mathrm{W/(m\times{}^0C)}$
porous matrix	porosity	0.1
	permeability	$10^{-14}\,\mathrm{m^2}$
	Specific heat	$815\,\mathrm{J/(kg\times{}^0C)}$
	thermal conductivity coefficient	$3.35\,\mathrm{W/(m\times{}^0C)}$

the top and the bottom of the computational domain are 0°C and 250°C respectively. Both the top and the bottom of the computational domain are impermeable in the vertical direction, while all the four side boundaries of the computational domain are assumed to be insulated and impermeable in the horizontal direction.

Figures 2.13 and 2.14 show the numerical and analytical solutions for the distributions of pore-fluid velocity and temperature in the axisymmetrical case (i.e. case 1) respectively. As expected, the numerical solutions for both pore-fluid velocity and temperature in this case are exactly axisymmetrical about the *y* axis. This implies that the three-dimensional problem considered in this particular case can be reasonably treated as a two-dimensional one. It is also observed that the numerical solutions in Fig. 2.13 compare very well with the previous solutions in Fig. 2.14

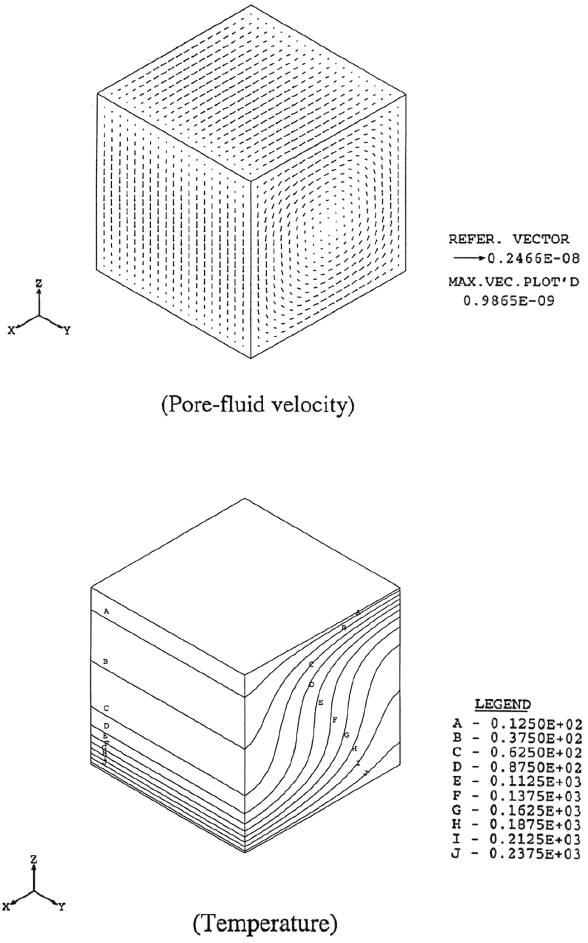

Fig. 2.13 Distributions of pore-fluid velocity and temperature in the porous medium (Case 1, numerical solutions)

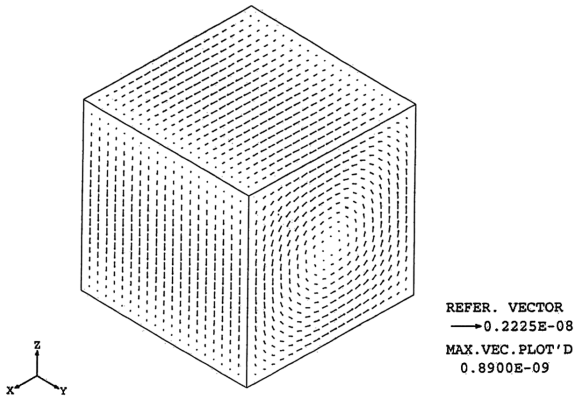

(Pore-fluid velocity)

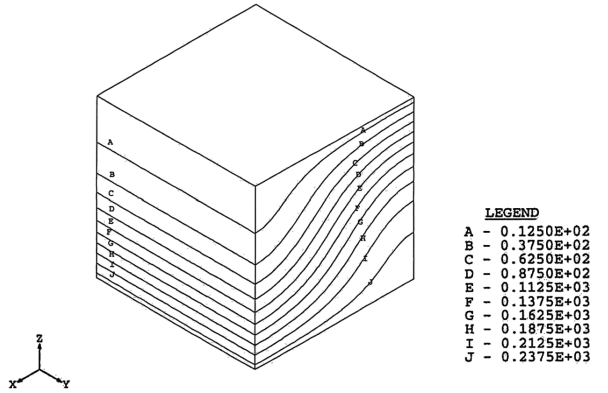

(Temperature)

Fig. 2.14 Distributions of pore-fluid velocity and temperature in the porous medium (Case 1, Analytical solutions)

for the axisymmetrical convective pore-fluid flow problem (Zhao et al. 1997a). This indicates that the progressive asymptotic approach procedure, although it was previously developed for the finite element modelling of two-dimensional convective pore-fluid flow problems, is equally applicable to the finite element modelling of three-dimensional convective pore-fluid flow in fluid-saturated porous media when they are heated from below.

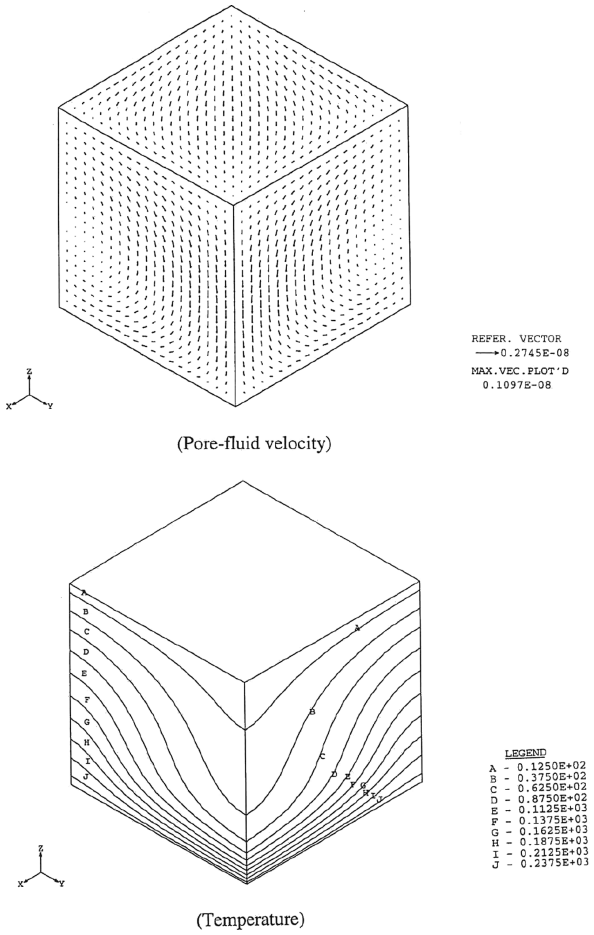

Fig. 2.15 Distributions of pore-fluid velocity and temperature in the porous medium (Case 2)

Figure 2.15 shows the numerical solutions for the distributions of pore-fluid velocity and temperature in the real three-dimensional case (i.e. case 2). By comparing the numerical solutions from case 1 (Fig. 2.13) with those from case 2 (Fig. 2.15), it is observed that the distribution patterns of both pore-fluid velocity and temperature are totally different for these two cases. This demonstrates that the perturbation of gravity at different planes may have a significant effect on the pattern of convective pore-fluid flow in three-dimensional hydrothermal systems. Just like two-dimensional convective flow problems, the solution dependence of three-dimensional convective flow on the direction of the perturbation of gravity need to be considered when these kinds of results are interpreted.

To further observe the movements of pore-fluid particles, the particle tracking technique introduced in this section is used during the numerical computation.

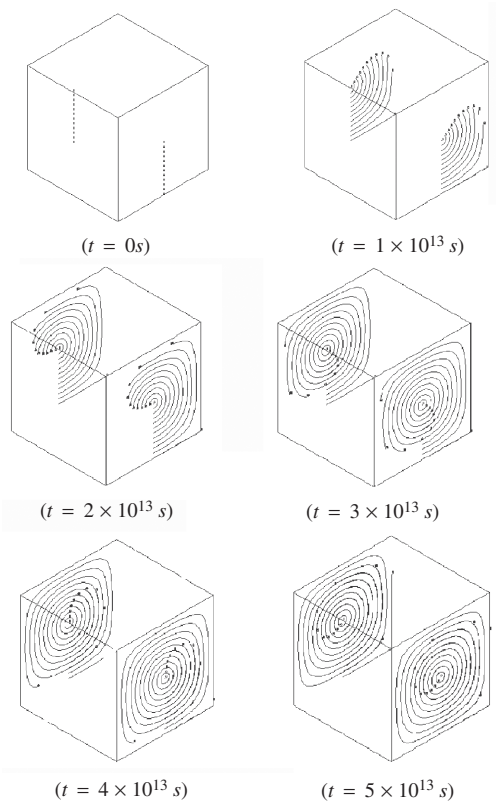

Fig. 2.16 Particle trajectories in the porous medium (Case 1)

We selected 24 particles, 12 of which are in the front plane and the rest are in the back plane of the computation domain, to view the trajectories of those particles. Figure 2.16 shows the particle trajectories in the porous media for several different time instants in case 1. It is clear that in this case, all the particles move within the planes they are initially located within (at $t = 0\,s$), because the convective pore-fluid flow (in case 1) is essentially axisymmetrical about the rotation axis of these particles considered. Figures 2.17 and 2.18 show the particle trajectories in the porous media for several different time instants in case 2. It is observed that the particle trajectories shown in case 2 are totally different from those shown in case 1, although the initial locations (at $t = 0\,s$) of these 24 particles are exactly the same for these two cases. In fact, the particle trajectories shown in case 2 are much more complicated than those shown in case 1. Since pore-fluid is often the sole agent to carry the minerals from the lower crust to the upper crust of the Earth, the different patterns of particle trajectories imply that the pattern of ore body formation and mineralization may be totally different in those two three-dimensional hydrothermal systems.

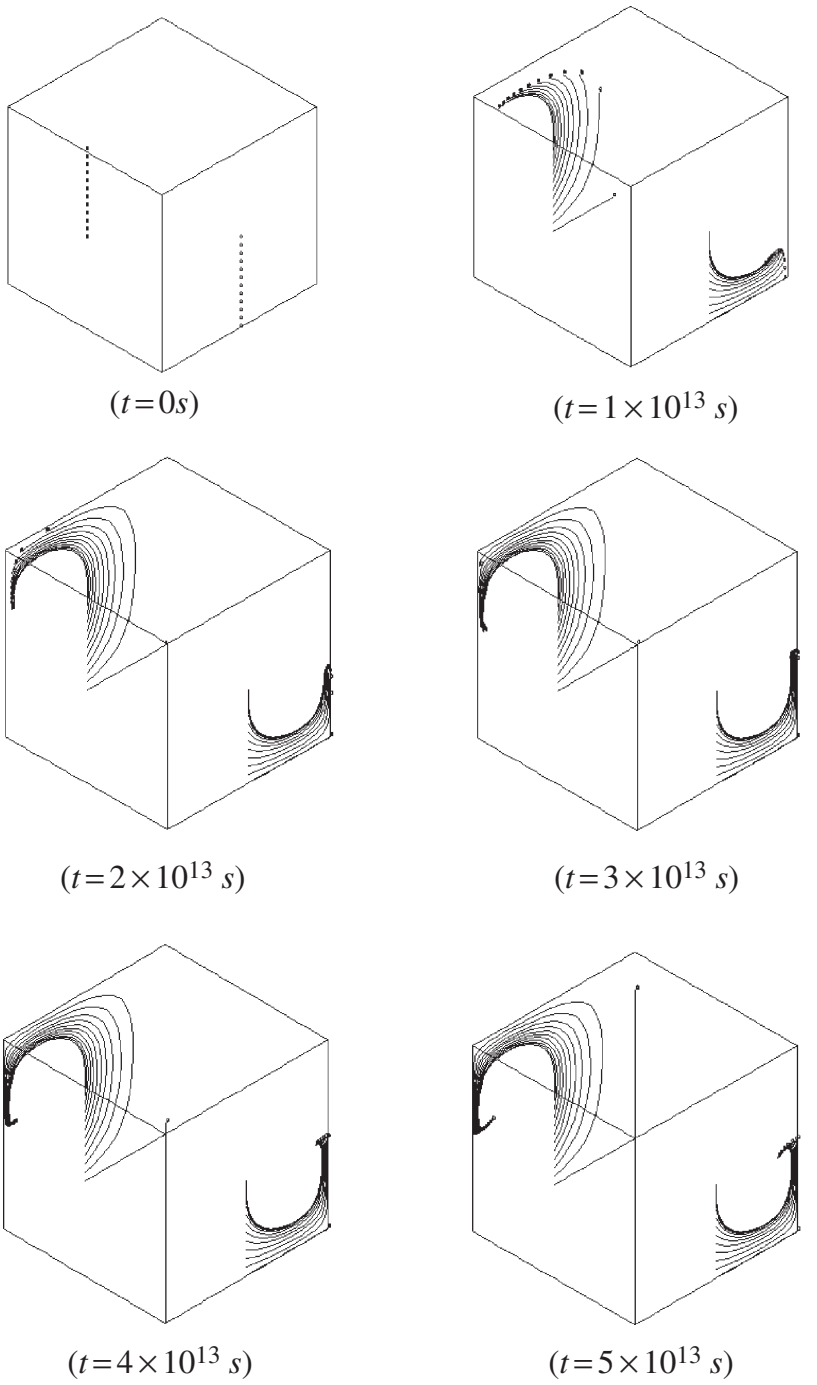

Fig. 2.17 Particle trajectories in the porous medium (Case 2)

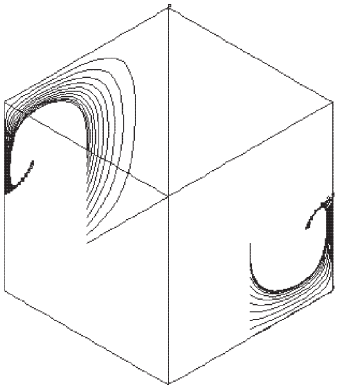

$(t = 6 \times 10^{13}\ s)$

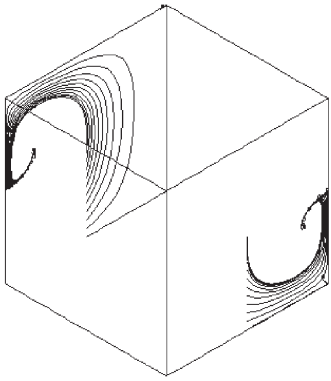

$(t = 7 \times 10^{13}\ s)$

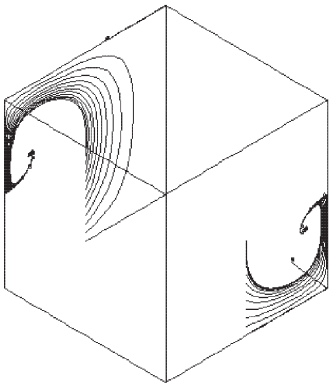

$(t = 8 \times 10^{13}\ s)$

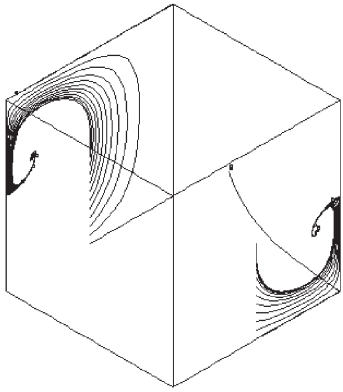

$(t = 9 \times 10^{13}\ s)$

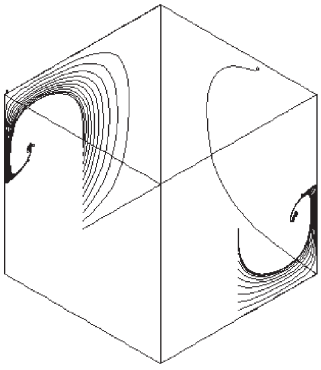

$(t = 1 \times 10^{14}\ s)$

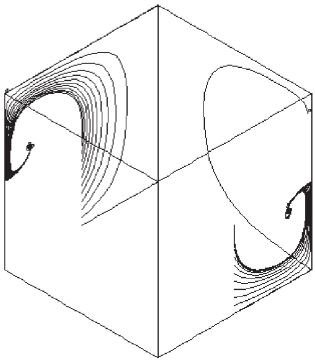

$(t = 1.1 \times 10^{14}\ s)$

Fig. 2.18 Particle trajectories in the porous medium (Case 2)

http://www.springer.com/978-3-540-89742-2

Fundamentals of Computational Geoscience
Numerical Methods and Algorithms
Zhao, C.; Hobbs, B.E.; Ord, A.
2009, XVI, 241 p., Hardcover
ISBN: 978-3-540-89742-2